Energy Conversion and Management: X 24 (2024) 100808

Contents lists available at ScienceDirect

Energy Conversion and Management: X

journal homepage: www.sciencedirect.com/journal/energy-conversion-and-management-x

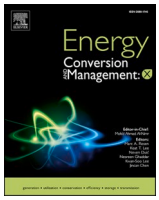

Identification and control of hydrothermal carbonisation process with energy consumption assessment

Riku-Pekka Nikula [a,*], Sajad Ahmadi [b], Velma Beri Kimbi Yaah [b], Hafiz Haq [c], Ville Tuomi [c], Mika Ruusunen [a]

[a] Control Engineering, Environmental and Chemical Engineering, University of Oulu, P.O.Box 4300, FI-90014 Oulu, Finland
[b] Environmental and Chemical Engineering, University of Oulu, P.O.Box 4300, FI-90014 Oulu, Finland
[c] School of Technology and Innovations, Industrial Management, University of Vaasa, P.O.Box 700, FI-65200 Vaasa, Finland

ARTICLE INFO

Keywords:
Energy consumption
Hydrothermal carbonisation
Model predictive control
Process simulation
System identification

ABSTRACT

The sustainable and cost-effective production of hydrochar requires energy efficient processing. In this study, data collected from laboratory-scale hydrothermal carbonisation experiments were used to identify dynamic models to predict reactor temperature based on estimated heating power. The performance was then analysed through process simulations with model predictive control. The optimal control model exhibited root mean squared error (*RMSE*) in the range of 3.19–11.47 °C in model validation with data sets of 31 experiments, whereas for process models it was 1.49–4.79 °C using their training data. In simulations with the optimal control model at the target temperatures of 180–200 °C for 4–6 h, the optimal mean values of mean absolute percentage error (*MAPE*), overshoot, and specific energy consumption were 0.56%, 2.50 °C, and 40.86 kWh/kg, respectively. Simulations indicated also that strict temperature control settings (average standard deviation $s = 1.24$ °C at target temperature) increased specific energy consumption slightly ($\bar{x} = 4.4\%$) when compared with control settings that allowed higher variance around a setpoint ($s = 5.11$ °C). However, the energy consumption was generally more dependent on the target temperature and processing time, which was also validated based on the measurements of 23 additional experiments. The presented dynamic modelling approach enables accurate real-time process control and predictive energy consumption optimisations for hydrothermal carbonisation.

1. Introduction

In hydrothermal carbonisation (HTC), biomass is heated under the subcritical conditions of water to temperatures typically around 180–260 °C in a closed vessel for several hours [1–3]. At the same time, the reaction pressure builds up in hot saturated water [4]. The biomass material reacts in an overall exothermic process with various complex simultaneous chemical reactions [5], which are governed by process parameters [6]. The outputs of reactions include solid and liquid phases and a small amount of gas, such as carbon dioxide [7]. The solid product, commonly known as hydrochar, can be used in various applications, such as soil amendment [8], water treatment [9], carbon sequestration [10], and more [11,12]. HTC does not require the drying of feedstock (wet biomass), which makes it promising from the economic perspective [2]. Actually, the energy efficiency of the process is an important and current topic [13–15], and many recent studies have highlighted that the economic performance of other industrial processes could also benefit from the integration with HTC [16–18].

During the process, energy is consumed to heat water and biomass from room temperature to target temperature, to heat the reactor walls, and due to energy losses [13]. Although heat is released via exothermic reactions, external energy is required to sustain the conversion process in practice [19]. Especially in a laboratory setup, relatively high amount of energy may be consumed to heat the thick reactor walls [13,20]. The minimisation of reactor energy losses could reduce the heating requirement after the initial heating phase [7,20]. Moreover, the energy efficiency could be increased by recovering energy and by using it to preheat the biomass-water mixture or to dry the hydrochar, especially in industrial scenarios [13]. Recent studies have also focused on the energy content of hydrochars and their relation to feedstock properties, process settings, and energy consumption during processing [20–23]. However, the dynamic modelling of process conditions and energy consumption during processing appears rare [24], even though such models can help to achieve energy efficient operation [25].

* Corresponding author.
E-mail address: riku-pekka.nikula@oulu.fi (R.-P. Nikula).

https://doi.org/10.1016/j.ecmx.2024.100808
Received 7 August 2024; Received in revised form 22 November 2024; Accepted 22 November 2024
Available online 24 November 2024

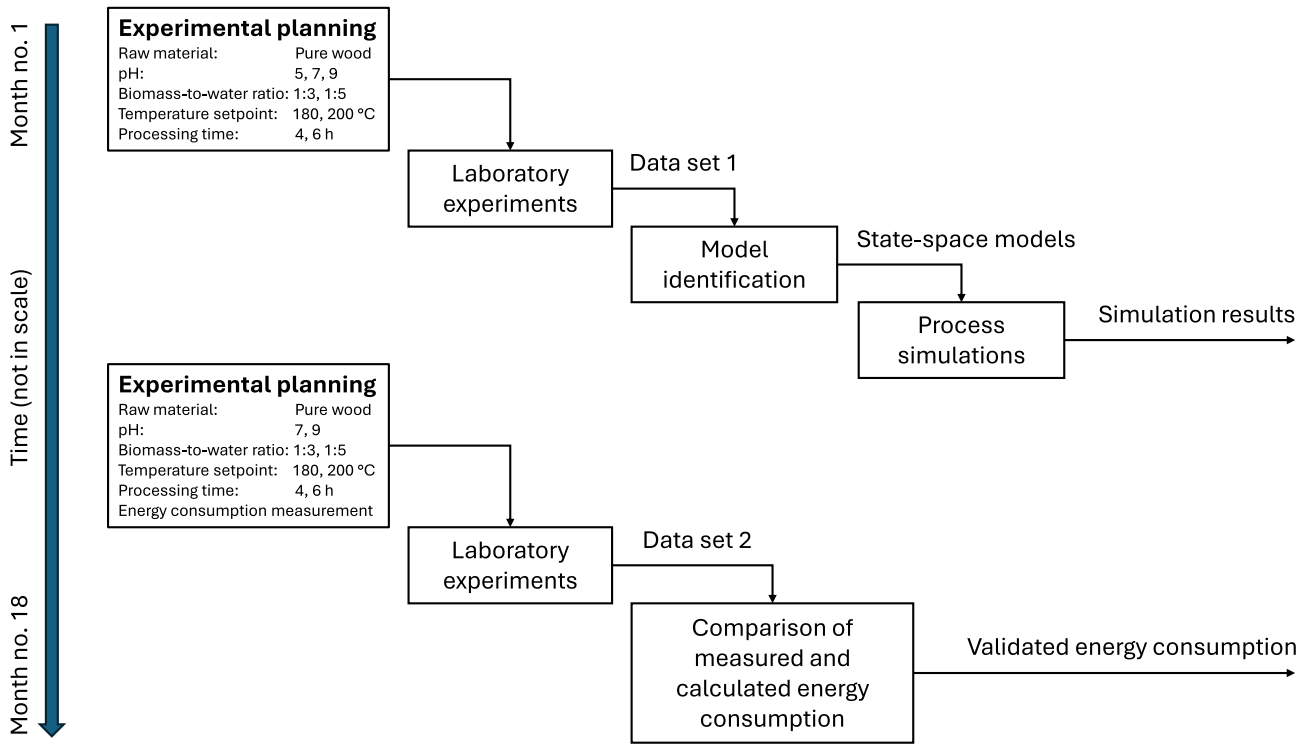

Fig. 1. General overview of research procedure.

The optimal process conditions in HTC are dependent on the feedstock properties and the desired hydrochar properties [26]. For example, the solid yield, H/C ratio, and O/C ratio of the product are inversely related to process temperature [6]. Increasing reaction temperature and time generally increases hydrochar energy content [22] but can reduce its energy yield [27]. Long reaction time increases the carbon content but decreases H/C and O/C ratios of the hydrochar, and so on [6]. Biomass-to-water ratio [28] and pressure [6] can affect the processing and products as well.

Recently, mathematical correlations have been identified in many studies between the process conditions and the properties of feedstocks and products. For example, Gallifuoco et al. [29] modelled the connections between the liquid and solid phase properties, whereas Sermyagina et al. [30] identified mathematical correlations between the process settings and the mass and energy yields of hydrochar samples. Li et al. [22] used feedstock properties in random forest models to predict the total energy recovered in hydrochars. The correlations are commonly identified by applying multivariate data-driven models, where multivariate linear regression [3,27,28], regression trees [31,32], random forests [22,33], artificial neural networks [34,35], and extreme gradient boosting [36] are some of the applied model structures. Although such static models help to understand the correlations in the process, dynamic models could represent its performance more realistically [37]. Then again, the detailed modelling of reaction kinetics and transfer phenomena is complicated due to the complexity of the reaction mechanisms and the richness of experimental conditions [24], even though rather comprehensive mathematical models have been presented by Heidari et al. [21], for example. In addition, heating modelling can help to understand the power requirements of the process [38], and lead the way to achieve the desired hydrochar properties energy-efficiently.

This study is focused, firstly, on the identification of models that capture the dynamics between the heating power and reactor temperature. The identification was done based on process data acquired during laboratory experiments, by identifying discrete-time state-space models [39]. Secondly, these models were used in process simulations to predictively control HTC process, with aims such as small tracking error and low energy consumption. In previous literature, the control of HTC reactor has been simulated and tested by applying an on–off controller by Heidari et al. [21]. Saha et al. [40] used a proportional-integral-derivative (PID) controller in their laboratory experiments. In this study, however, model predictive control (MPC) was applied in the simulations because it is often the preferred control choice in modern industrial applications [41]. Furthermore, the simulations were performed in a scenario where the process was different from the control model, by using different process models, i.e., by generating a plant-model mismatch [42] to open the potential of this approach also for practical applications.

To summarise, the main novelties presented in this paper include:

- data-driven identification of dynamic models for HTC process,
- assessment of energy consumption in HTC based on process control values,
- analysis of energy consumption and control performance by simulating with the models identified.

2. Materials and methods

Fig. 1 illustrates the steps of this work, which were conducted in two parts. The upper part shows the steps of modelling and simulation work, whereas the lower part illustrates the steps for validating the energy consumption assessment method. In addition, the following sub-sections disclose the applied research methods and materials more comprehensively. The first sub-section describes the hydrothermal carbonisation experiments and data sets used. The second sub-section describes the applied modelling and simulation procedures.

2.1. Hydrothermal carbonisation experiments

2.1.1. Pretreatment of raw material

In this study, construction wood waste (pure Class A wood) was used as the raw material. The wood was collected from Kiertokaari (Oulu,

Table 1
Synthesis conditions varied during the HTC experiments.

Parameter	Values
Temperature (°C)	180, 200
Time (h)	4, 6
pH	5, 7, 9
Biomass-to-water ratio	1:3, 1:5

Finland). It was chopped into 10–20 mm sizes and crushed using a Rapid 200 Series granulator. The granulator was manually operated by feeding pure wood into the container, which then dropped the material onto rapidly rotating knives. The crushed material passed through an adjustable screen with varying sizes (1 to 5 mm), and the resulting product was collected into bags. There was no drying of raw materials prior to the HTC process.

2.1.2. Hydrothermal carbonisation

The hydrothermal carbonisation was done with a high-pressure Parr reactor (4575/76 HP/HT Pressure Reactors, USA) equipped with a 4848-reactor controller and 1.8 kW heater. HTC was done under different conditions that are presented in Table 1. About 45.5 g of pure wood and distilled water based on the selected biomass-to-water ratio were put in the reactor. About 30% of air space was maintained in the reactor. Throughout the process, both the temperature (Type J thermocouple, ±2 °C accuracy) and pressure were actively monitored using the 4848-reactor controller and the pressure gauge (1% FS accuracy) installed at the top of the reactor. The HTC process was carried out at 180 °C and 200 °C for 4 and 6 h. The pressure varied (10–20 bars) according to the processing temperature. Cooling water was used to prevent the reactor from overheating. Once the system naturally cooled down, vacuum filtration was used to separate the hydrochar from the liquid phase and dried in an oven at 80 °C for 24 h. Each experiment was conducted three times to minimize experimental error and enhance the reliability of the results. In addition, electricity consumption was measured by FHT-9999 Energy Meter, the accuracy of which was studied by Liikkanen and Nieminen [43]. The schematic and cross-section views of the reactor are illustrated in Fig. 2.

2.1.3. Data sets

Two data sets were collected for analysis. Data set 1 was acquired for model identification and simulation. Data set 2 included energy consumption measurements that were missing from the first set. Therefore, the second set was used to validate the calculated energy consumption, described in Section 2.2.3. Both sets were used for the statistical analysis of calculated energy consumption in relation to process parameters as well. From the perspective of energy consumption, the main process parameters were assumed to be the processing time (t) and the temperature setpoint (T), which are presented in Table 2 for different experiments analysed. All process settings and the dry mass of produced hydrochar are shown in Appendix A.

Fig. 3 illustrates the reactor temperature, the control loop output, and the calculated energy consumption in experiment 1, where the temperature setpoint was 200 °C and it was held four hours, as shown in Table 2. In the start, the reactor was heated with high power for several minutes. The temperature reached the setpoint at the 52-min point, as shown in graph (a). Thereafter, the controller varied its output in the range of 0–100 to keep the temperature around the setpoint, as shown in graph (b). The heating-related energy consumption was thus assumed periodic as shown in graph (c). The experiment ended when four hours of processing around the target temperature was reached. In the other experiments, the process was operated similarly. However, each experiment resulted in a slightly different operation, even with the same process settings.

2.2. Model identification and control

2.2.1. State-space modelling

A common way to represent a linear system in practice is to use state-space models and difference equations [44]. A linear time-invariant and discrete-time system can be described as

$$x(k+1) = Ax(k) + Bu(k) \tag{1}$$

$$y(k) = Cx(k) + Du(k) \tag{2}$$

Table 2
Categorisation of experiments in data set 1 ($n = 31$) and data set 2 ($n = 23$) based on processing time (t) at setpoint temperature and setpoint temperature (T).

Setting (no., t, T)	Data set 1, experiments	Data set 2, experiments
1. $t = 4$ h, $T = 180$ °C	4, 5, 6, 12, 13, 14, 26, 27, 28	37, 38, 39, 40, 41, 42, 43, 44, 45
2. $t = 4$ h, $T = 200$ °C	1, 2, 3, 15, 16, 17, 29, 30, 31	32, 33, 34, 35, 36, 46, 47, 48
3. $t = 6$ h, $T = 180$ °C	7, 8, 9, 10, 11	52, 53, 54
4. $t = 6$ h, $T = 200$ °C	18, 19, 20, 21, 22, 23, 24, 25	49, 50, 51

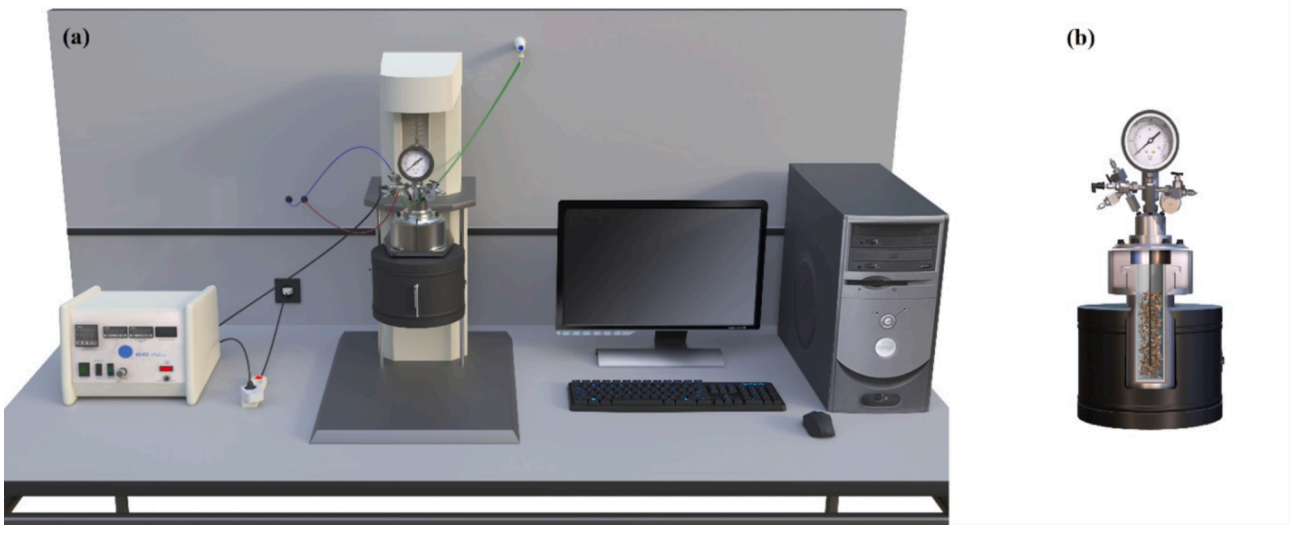

Fig. 2. (a) Schematic view of the Parr reactor and 4848-reactor controller connected to a computer (b) cross section view of the reactor with the sample inside.

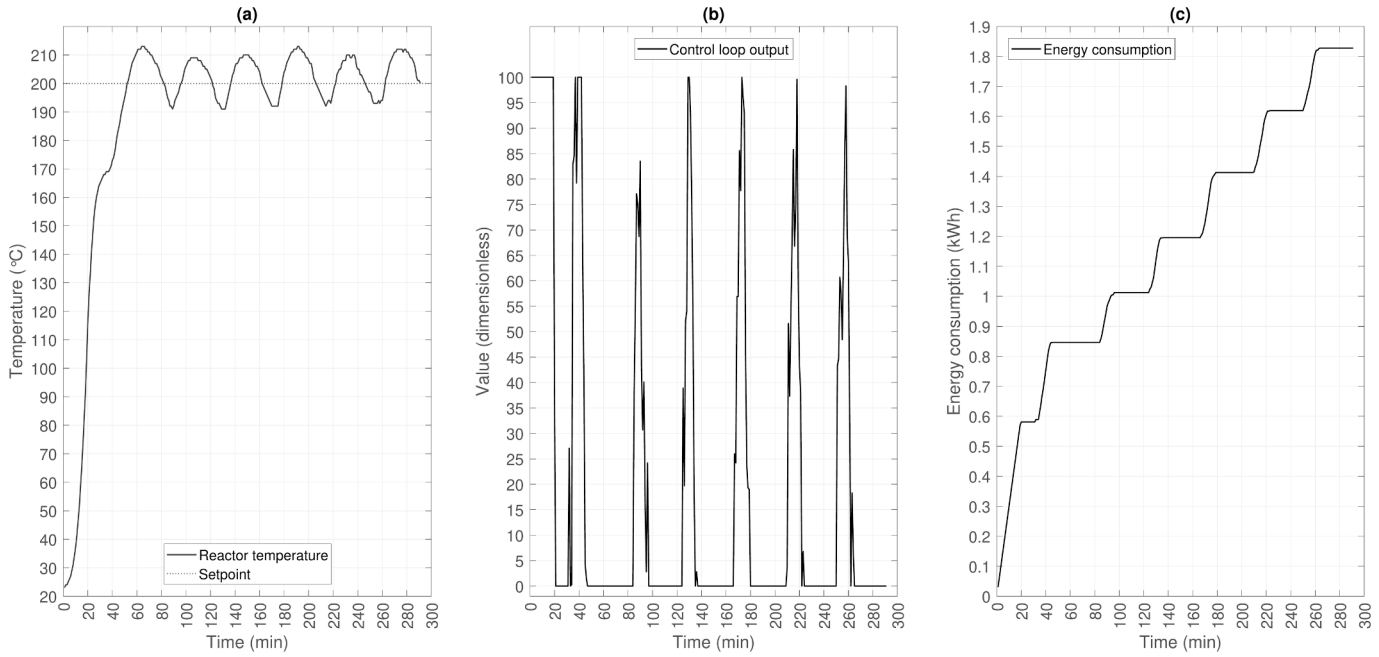

Fig. 3. Time series examples for main process variables measured during experiments: (a) reactor temperature, (b) control loop output, and (c) energy consumption calculated based on control loop output.

where x is the state vector, u is the input vector, and y is the output vector. For a system with single input and single output, the matrices A with size n-by-n, B (n-by-1), C (1-by-n), and D (1-by-1) represent the state, input, output, and feedthrough matrices, respectively. This state representation describes an n^{th} order linear physical system as a set of first-order difference equations in a matrix format. In this study, the model input u was the control loop output, and the model output y was the reactor temperature, which are illustrated in Fig. 3.

By using N4SID (numerical algorithm from subspace system identification) algorithms, the model identification can be done quickly based on time series data [25]. Such algorithms are non-iterative and overcome the disadvantages of iterative algorithms, such as the sensitivity to initial estimates, local minima of the objective criterion or unsuccessful convergence [39]. In this study, MATLAB® function *n4sid* was used, where the parameters defined by the user included the model order (*NX*) in the range 1–10, and the weighting scheme (*N4Weight*), where '*CVA*' [45], '*SSARX*' [46] and '*MOESP*' [47] were applied.

2.2.2. Model predictive control

Model predictive control is the class of advanced control techniques most widely applied in the process industries [48]. MPC applies a model for predicting future process values and to calculate future controller outputs to obtain the optimal output trajectory for the setpoint tracking or reference trajectory tracking [49]. The main components of MPC include a dynamic process model, constraints, and an optimisation algorithm. The control actions are commonly defined by numerically solving a quadratic programming problem in real-time, at each time step [50].

MPC has various tuneable parameters, such as the lengths of prediction and control horizons and the weights on controlled and manipulated variables [49]. Additionally, constraints can be used to limit the values of variables during optimisation. A relatively vast literature on MPC is available for additional reading from different perspectives, such as the review article by Schwenzer et al. [41] on the practical application or the guidelines by Alhajeri and Soroush [49] on parameter tuning.

The quadratic cost function, which was continuously optimised in the process simulations, can be written as

Table 3
Applied parameter values in MPC.

Parameter	Values
ne(min)	6, 8, 10, 12, 14, 16, 18, 20
w_o(dimensionless)	0.2, 0.4, 0.6, 0.8, 1, 1.5
w_{mr}(dimensionless)	0.1, 0.5, 1

$$J(k) = w_o \sum_{i=1}^{ne} \left(y_s(k+i) - \hat{y}(k+i)\right)^2 + w_{mr} \sum_{j=1}^{nu} \Delta u(k+j-1)^2 \tag{3}$$

where w_o is the output weighting factor for control error, w_{mr} is the input weighting factor for the control increments, Δu is the control increment, ne is the prediction horizon length, nu is the control horizon length, and k is the current discrete time step. The control value which is updated each time step is $u_k = u_{k-1} + \Delta u$. Parameter y_s is the setpoint for the controlled variable y and its prediction is $\hat{y}$. Various values for parameters w_o, w_{mr}, and ne were tested in this study, as shown in Table 3. The control horizon length was fixed to $nu = 2$ (min). The applied constraints for process variables were $u \in [0, 100]$ and $y \in [0, 1.1 \times y_s]$ °C.

In practical applications, the process and its model commonly have some level of mismatch [51]. Therefore, the predicted values and the corresponding measured values may deviate, generating an offset between the desired and actual values of the controlled variable [50]. Different methods to offset-free tracking, such as learning-based MPC [52], input adaptation [42], and disturbance rejection [53] have been proposed but a "standard practice" method is missing [50]. In this study, a simple method was used, where disturbance values were added to the model output value (2) in the control model. In this case, the output equation in the controller became

$$\hat{y}(k) = Cx(k) + Du(k) + d \tag{4}$$

where d is a constant value used across the prediction horizon. It is defined by subtracting the model output from the measured output at the current step k. In practice, this means that the model output at the current step k is first calculated by using (2); the difference from the measured output, i.e., $d = y(k) - \hat{y}(k)$, is calculated thereafter; and

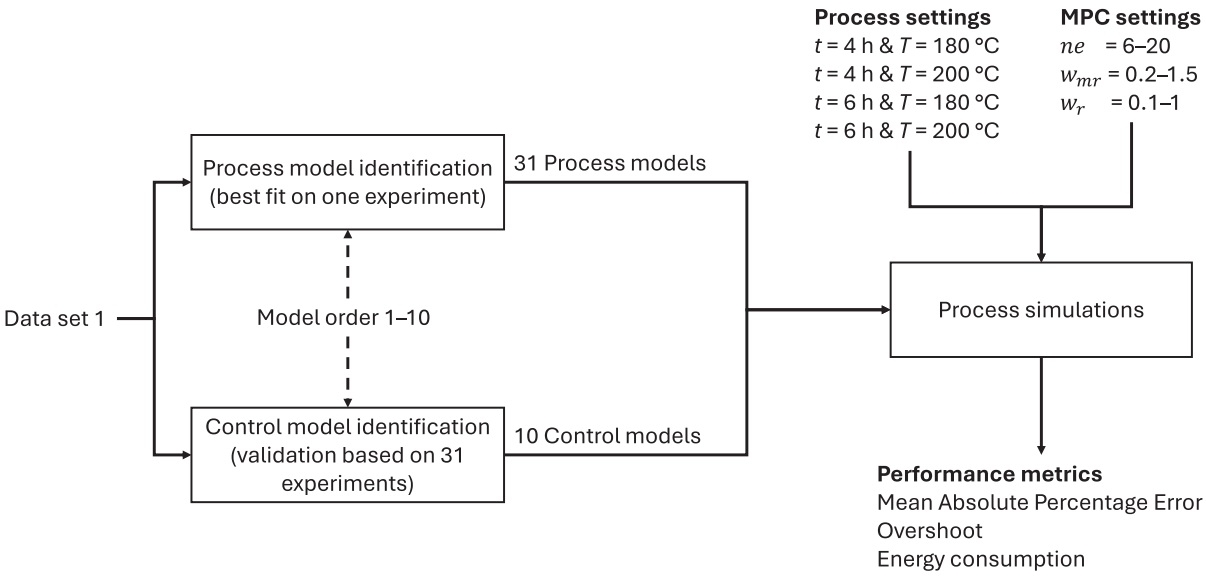

Fig. 4. Applied model identification and process simulation framework.

finally used as the disturbance d in (4) for the predictions during the optimisation.

2.2.3. Performance metrics

The prediction performance of state-space models was evaluated by using the root mean squared error (*RMSE*) which is given by

$$RMSE = \sqrt{\frac{1}{N}\sum_{i=1}^{N}(y_i - \hat{y}_i)^2} \tag{5}$$

where N is the total number of observations, y_i is the measured value and $\hat{y}_i$ is the predicted value of the model output. Moreover, mean absolute percentage error (*MAPE*) was used to measure the average deviation of the controlled variable from its setpoint, which can be described as

$$MAPE = \frac{1}{N}\sum_{i=1}^{N}\left|\frac{y_i - y_s}{y_s}\right| \times 100\% \tag{6}$$

In this case, it was calculated from the period that corresponded to the processing at target temperature, such as the period of 52–291 min in Fig. 3. In addition, overshoot (O) was used to measure the peak deviation from the setpoint within the same period. It is defined here as

$$O = \max_{i=1\cdots N}(|y_i - y_s|) \tag{7}$$

which in this case includes the maximum deviation to the negative di-

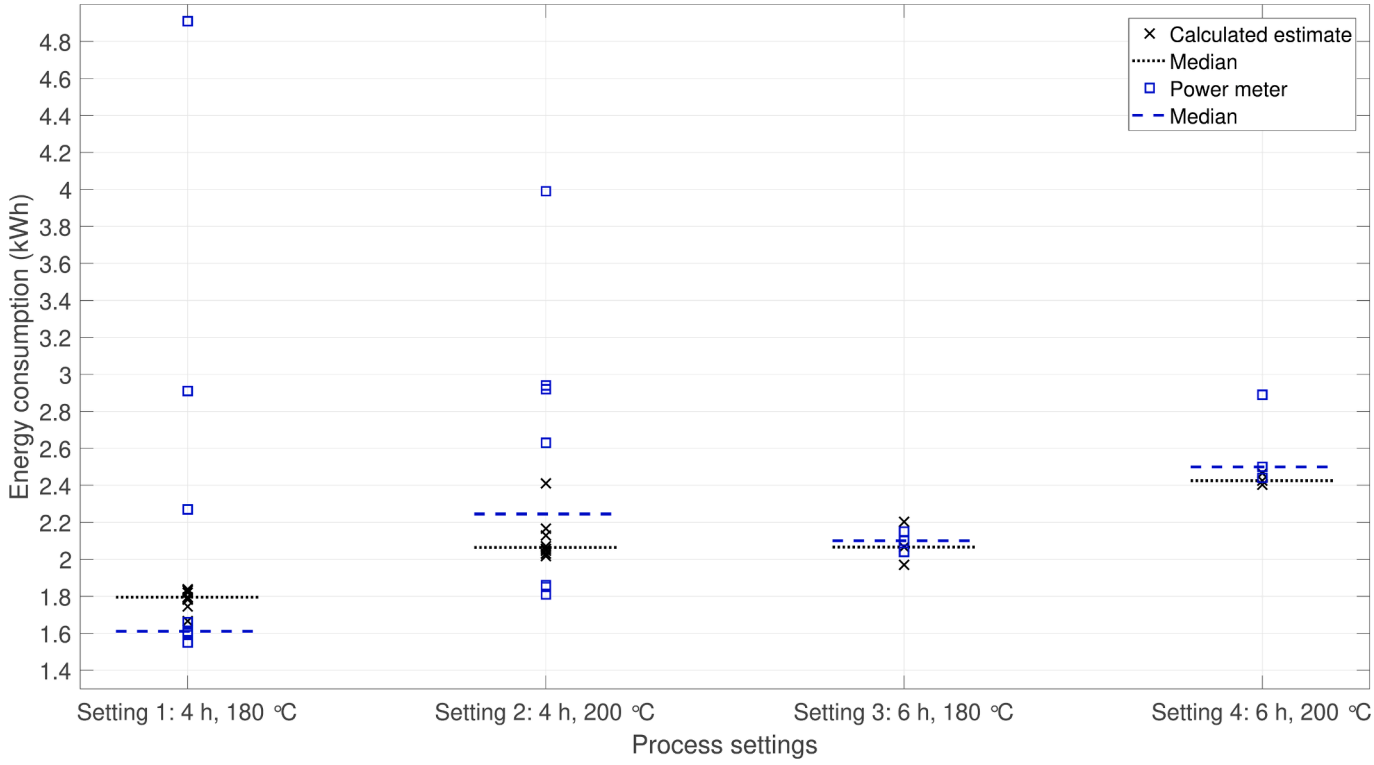

Fig. 5. Energy consumption in hydrothermal carbonisation of construction wood waste with different process settings.

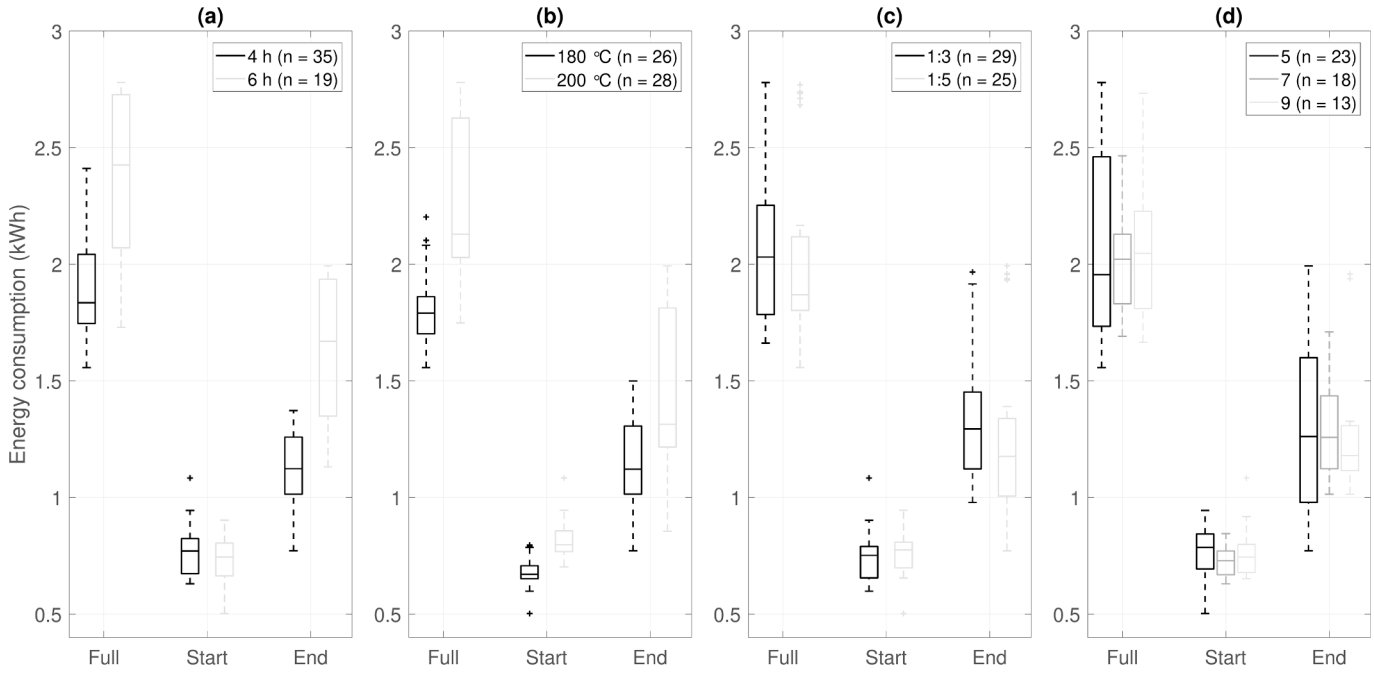

Fig. 6. Energy consumption in relation to (a) processing time, (b) temperature setpoint, (c) biomass-to-water ratio, and (d) pH setpoint. 'Full' shows the total energy consumption, 'Start' shows the consumption before the temperature setpoint was reached the first time, and 'End' is associated with the consumption after the setpoint was reached the first time.

rection, i.e., the undershoot as well. Finally, the calculated energy consumption (kWh) is defined here by

$$E = \sum_{i=1}^{N} \left(\frac{u_i}{100} \times P_{heater} \right) \div 60 \tag{8}$$

where u_i is the value of control loop output, in the range of 0–100 (dimensionless), P_{heater} is the maximum power of the heater (kW). In this study, a 1-min sampling interval was applied, and therefore, the sum was divided by 60 to obtain kilowatt-hours.

2.2.4. Modelling and simulation procedures

Models were identified for two purposes based on data set 1 described in Section 2.1.3. Firstly, separate process models were trained for all 31 experiments represented in the data set. Different orders and weighting schemes were tested for the models, as described in Section 2.2.1. The model that resulted in the lowest *RMSE* was selected to represent each experiment separately. The aim was to identify a model that would represent a specific full experiment as closely as possible with the selected input and output variables. These 31 models were then later used in simulations to represent the actual process in different experiments.

Secondly, ten control models were identified for MPC. The model training was done by using the data of a single experiment at a time. The model was then tested by using the data of all 31 experiments. Thereafter, data from another experiment were used for training another model and the model was tested by using the data of all 31 experiments, and so on. Based on this validation, the model that resulted in the lowest average *RMSE* was selected as the control model with the selected order. This was repeated with all model orders (1–10) separately.

The simulations were then performed with all the combinations of ten control models and 31 process models. In addition, the 144 combinations of parameter values in MPC, as shown in Table 3, were tested. This resulted in 44,640 simulation runs. The process settings, defined by the temperature setpoint and processing time, were the same as in the original 31 experiments, as shown in Table 2. The simulations provided information on the effects of control models and control parameters on the selected performance metrics. Fig. 4 illustrates the modelling and simulation procedures graphically.

3. Results and discussion

This section is divided into seven sub-sections. In the first sub-section, the energy consumption assessment method is validated based on the energy consumption measurements. Thereafter, the correlations are analysed between the energy consumption estimates and process parameters. The third sub-section focuses on model identification, while the fourth sub-section focuses on the control model selection and the effects of control parameters via exhaustive simulations. Thereafter, simulation cases are presented with optimised control parameters in two sub-sections. Finally, the significance of the results is discussed in the last sub-section.

3.1. Validation of calculated energy consumption

Fig. 5 illustrates the energy consumption during the laboratory experiments contained in data set 2 ($n = 23$) by showing the measured values (blue squares) and the calculated estimates (black crosses). Moreover, the experiments are categorized based on four process settings, as defined also in Table 2. The medians are shown for each setting as dotted lines.

Based on the medians, the relative differences between the calculated and measured energy consumptions were 11.5%, 8.1%, 1.6%, and 3.0% for process settings 1–4, respectively. This indicates that the measured and calculated values were relatively similar, especially in the 6-hour experiments. However, some measured values especially in the 4-hour experiments were exceptionally high when the heater power (1.8 kW) is considered. They can be explained by a malfunction in the power meter or operation that cannot be explained based on the control loop output u solely. Compared with the measurements, the calculated values were less scattered, perhaps showing the energy consumption associated with reactor heating more precisely.

The medians in Fig. 5 clearly show that the higher temperature setpoint and processing time resulted in higher energy consumption, as can

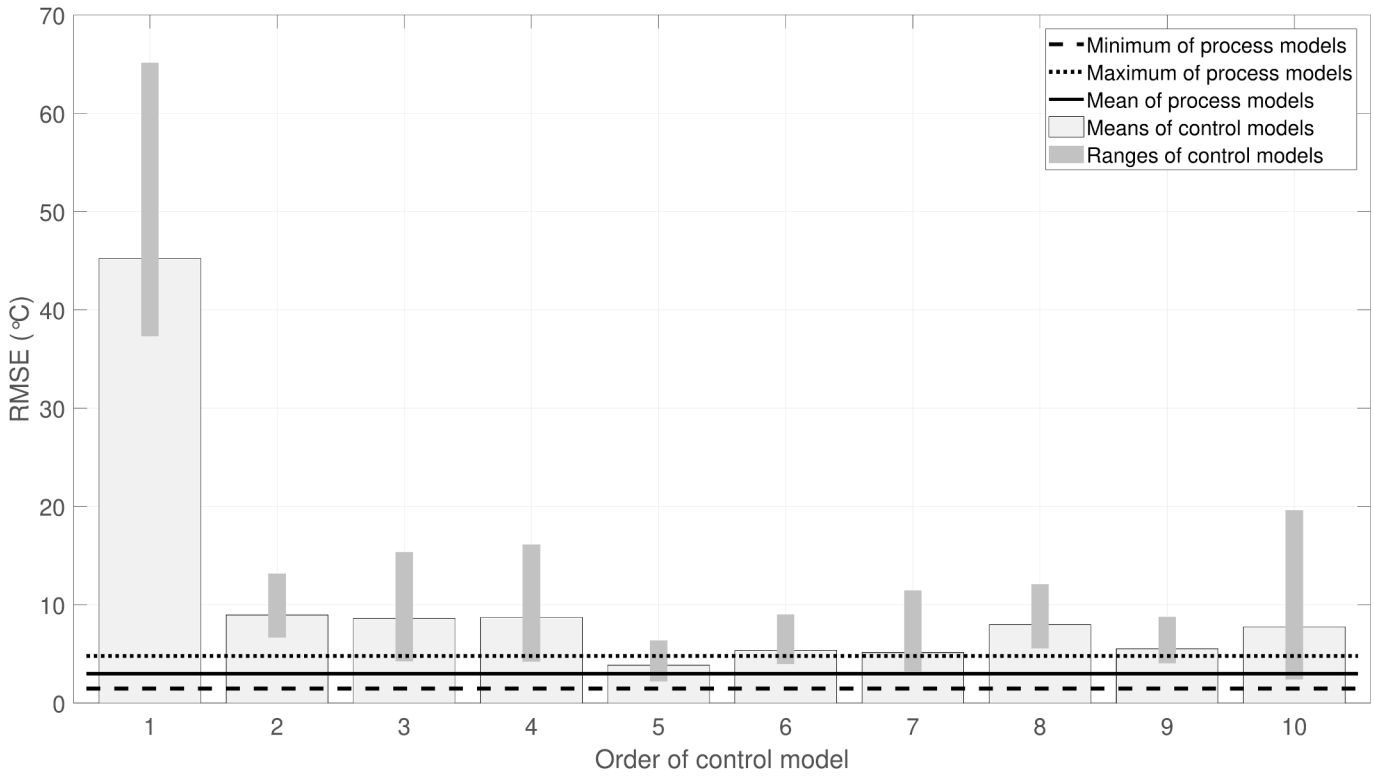

Fig. 7. Mean and range of *RMSE* for ten control models and 31 process models. The values for control models come from the validation based on the data of 31 experiments while the values for process models come from fitting them on their separate training data.

be logically expected. Then again, process settings 2 and 3 had almost the same consumption (almost 2.1 kWh) based on the medians of calculated estimates. The median of measured values was higher for setting 2 than for setting 3, which can be explained by the exceptionally high measured values recorded during the experiments. The full range of medians was 1.6–2.5 kWh for the measurements and 1.8–2.4 kWh for

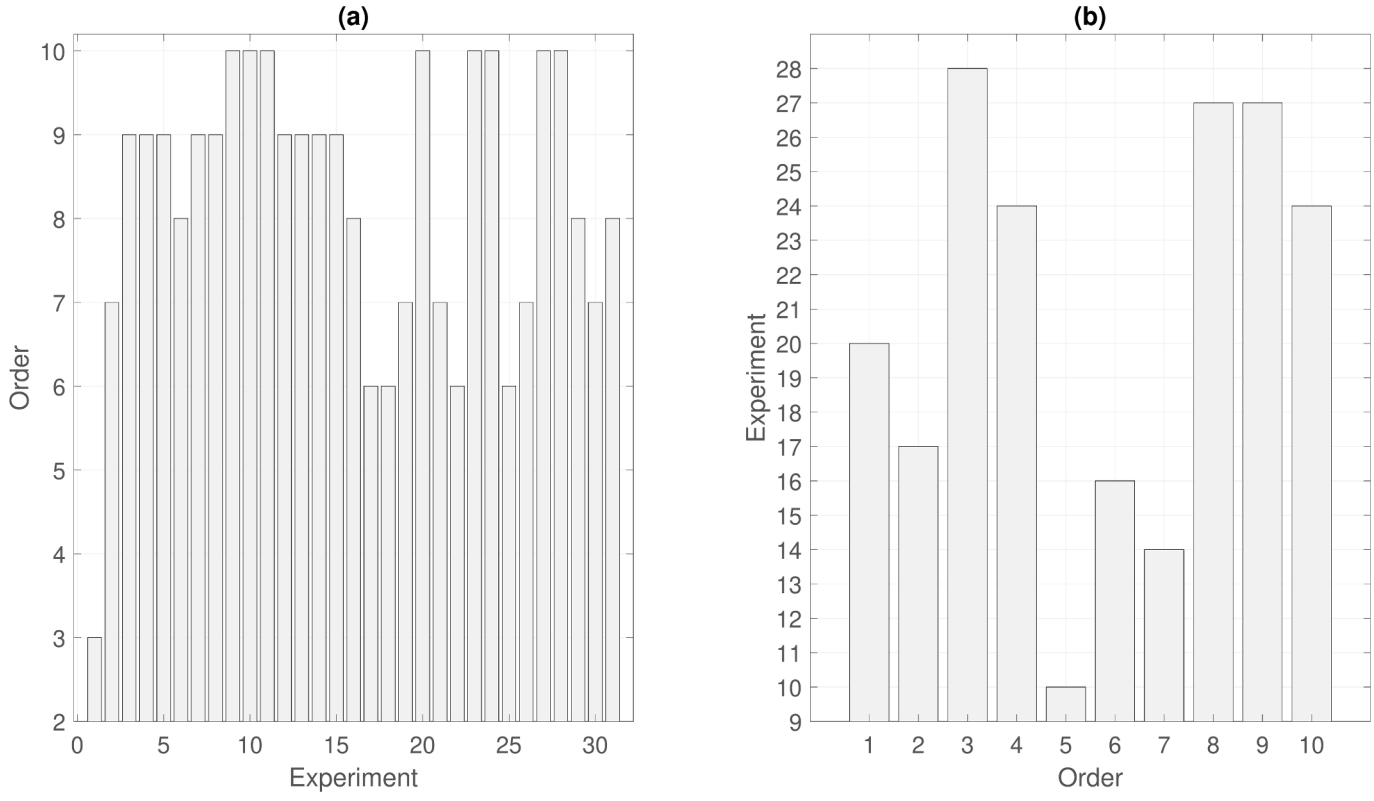

Fig. 8. (a) Orders of process models and (b) experiments used for control model identification.

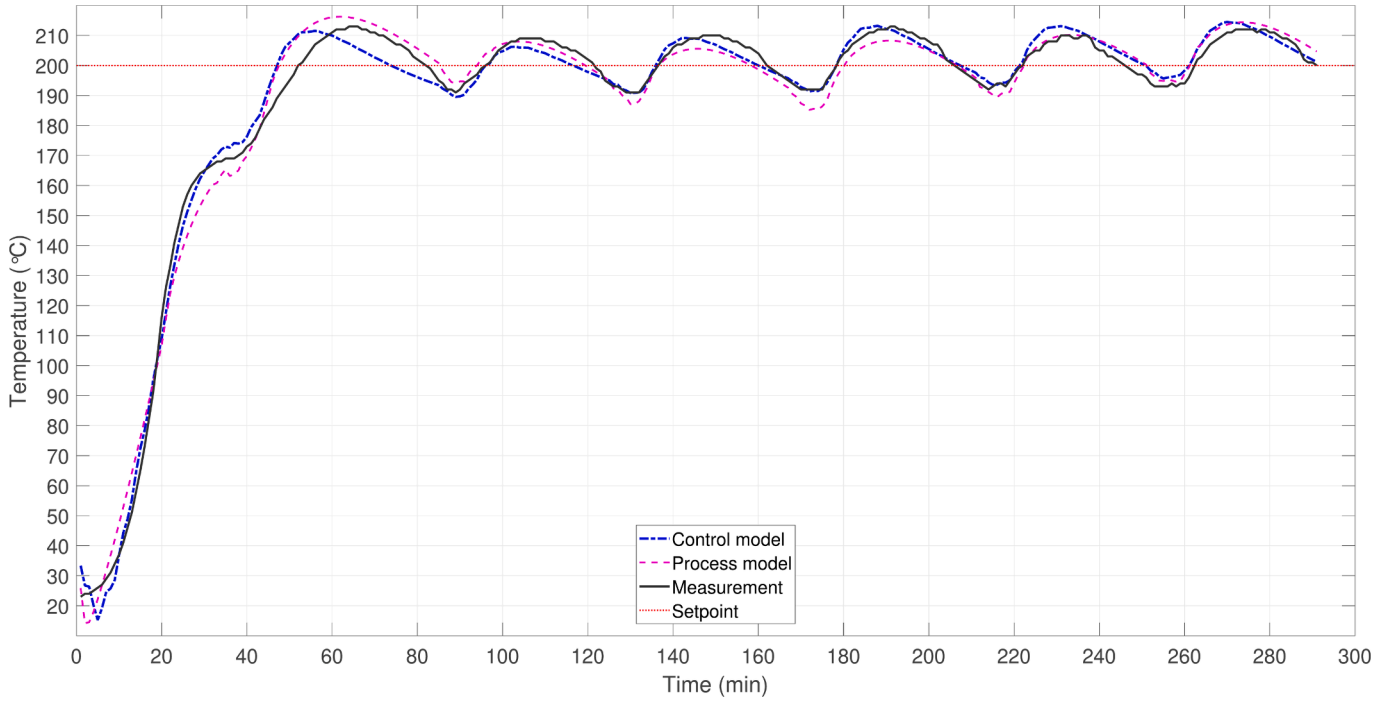

Fig. 9. Fitting of control model and process model on time series of experiment 1.

the calculated estimates. The maximum values were thus 56% and 33% higher than the minimum values, respectively. The process settings had a significant effect on the total energy consumption.

3.2. Correlations of experimental settings with energy consumption

Fig. 6 displays the calculated energy consumption as boxplots with different process settings (see Appendix A) by using the data from both datasets ($n = 54$). The boxes represent the interquartile range, the lines inside boxes represent medians, and the whiskers represent the range. The plus signs are outliers. MATLAB® *boxplot* function was used with the default settings. Graphs (a) and (b) are related to process conditions, i.e., the processing time and temperature, whereas graphs (c) and (d) are related to the characteristics of the processed material, such as the biomass-to-water ratio and pH. Each full experiment was also divided into two stages, which include the heating period before reaching the temperature setpoint and the processing period thereafter at the target temperature for many hours. Those are marked as 'Start' and 'End' in the graphs.

Graph (a) shows that the processing time had a strong effect on the total energy consumption and the energy consumption at the target temperature, as revealed by the nonoverlapping interquartile ranges of different processing durations. Then again, the temperature setpoint had a significant effect on the energy consumption at the start and the end of processing both, as shown in graph (b). At the target temperature, the energy consumption was higher in 200 °C than in 180 °C although the interquartile ranges are overlapping. At the start, the difference was more significant because the interquartile ranges are not overlapping.

Biomass-to-water ratio and pH did not have a distinguishable effect on energy consumption, which is shown by the overlapping boxplots in graphs (c) and (d), respectively. However, this analysis does not exclude the possibility that biomass-to-water ratio, for example, has some effect on the energy consumption in case the other process settings are set fixed. While these parameters did not show a strong correlation with energy consumption, excluding their effects from modelling and simulation seems reasonable.

3.3. Model identification

Fig. 7 shows the mean and range of *RMSE* in the validation of control models, based on data set 1. The lowest mean 3.86 °C, which corresponds to mean *MAPE* = 2.15%, was achieved with the model that had an order of five. The range was 2.19–6.38 °C. The poorest fit was achieved with the simplest model (order = 1) with the mean over 45 °C. In general, the models with the orders of 5–10 had lower mean than the models with lower orders. Perhaps it should be mentioned that *MAPE* in model identification was calculated based on the entire time series of the predicted and measured time series, which departs from the definition given in Section 2.2.3.

In addition, Fig. 7 shows the mean (2.99 °C), minimum (1.49 °C), and maximum (4.79 °C) *RMSE* of all 31 process models fitted on their training data. The corresponding values of *MAPE* were 1.68%, 0.85%, and 2.99%, respectively. These values were lower than the corresponding values with any control model, which is explained by the fact that the process models were only tested with their own training data. After all, the purpose was to use them as representatives of laboratory experiments as accurately as possible, and then use them as process models in simulations, where process and control models had mismatch.

Fig. 8 illustrates the model order for each process model in graph (a). The process models had often rather a high order ($\geq$6) and seventeen of them had the order of 9 or 10. This indicates that the best fit on training data was generally achieved with models that had many state variables. The experiments used for the training of the control models are shown in graph (b). The control model was identified twice based on experiment 24 ($t = 6$ h, $T = 200$ °C) and experiment 27 ($t = 4$ h, $T = 180$ °C). Based on the mean *RMSE* in validation, the best control model (order 5) was identified from 6-hours experiment in 180 °C temperature.

Fig. 9 demonstrates the fitted process model and control model (order 5) using the data of experiment 1 (see also Fig. 3). For this set of reactor temperature values, *RMSE* of the process and control models were 4.79 °C and 4.16 °C, respectively. The process model had the highest *RMSE* of 31 identified process models (see also Fig. 7), which indicates its fit was the poorest of all process models. The process model and the control model clearly had different performances with the same values of input u, which highlights the discussed need for mismatch

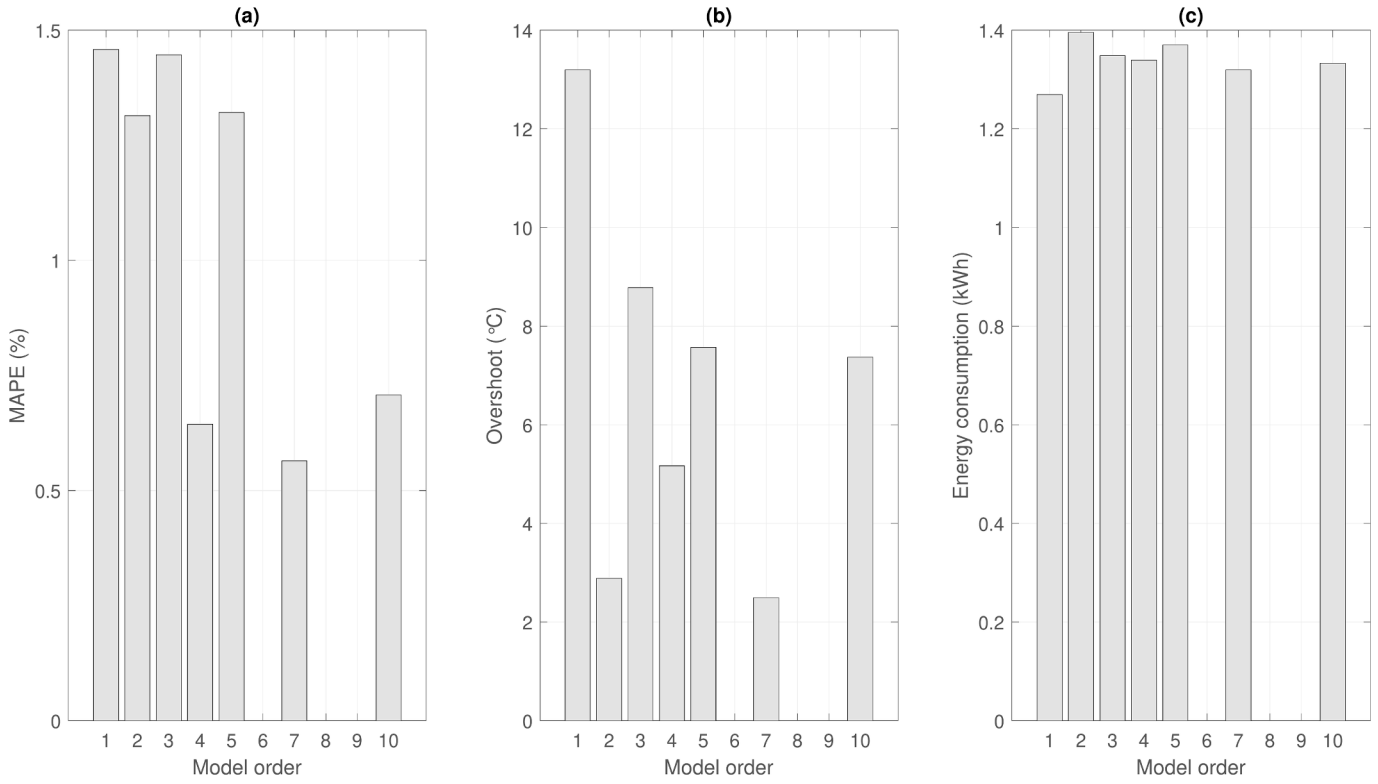

Fig. 10. (a) Minimum average *MAPE*, (b) minimum average overshoot, and (c) minimum average energy consumption at target temperature for each tested control model, based on simulations with 31 process models.

consideration in MPC. The estimated total energy consumption was 1.83 kWh (or 55.88 kWh for one kilogram of hydrochar produced) while the consumption at the target temperature was 0.98 kWh (30 kWh/kg).

3.4. Model selection and parameter effects on control

The control models were tested in exhaustive simulations, where the process data, i.e. the reactor temperature values (y), were generated by using the process models. The process model input (u), i.e. the control

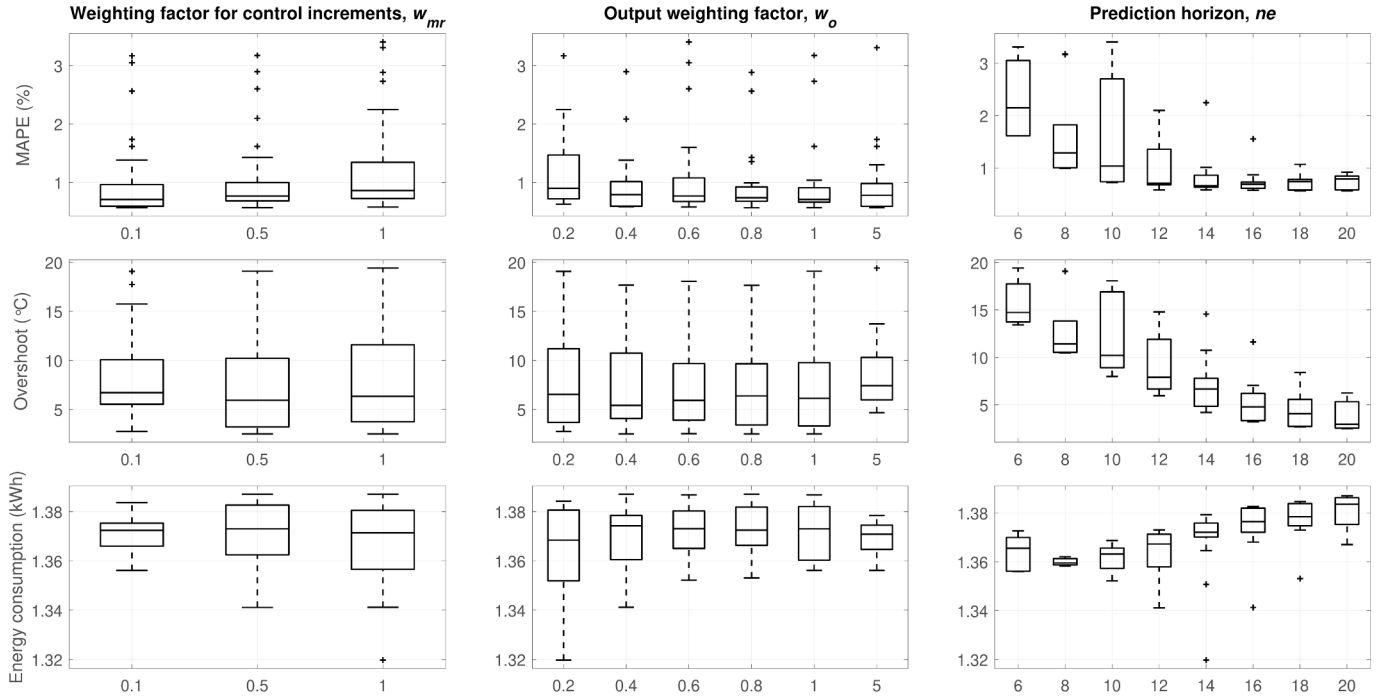

Fig. 11. Effect of control parameter values on performance metrics: The graphs from top to bottom show mean *MAPE*, mean overshoot, and mean energy consumption. The parameter values are shown on the horizontal axes for w_{mr} on the left, w_o in the middle, and ne on the right.

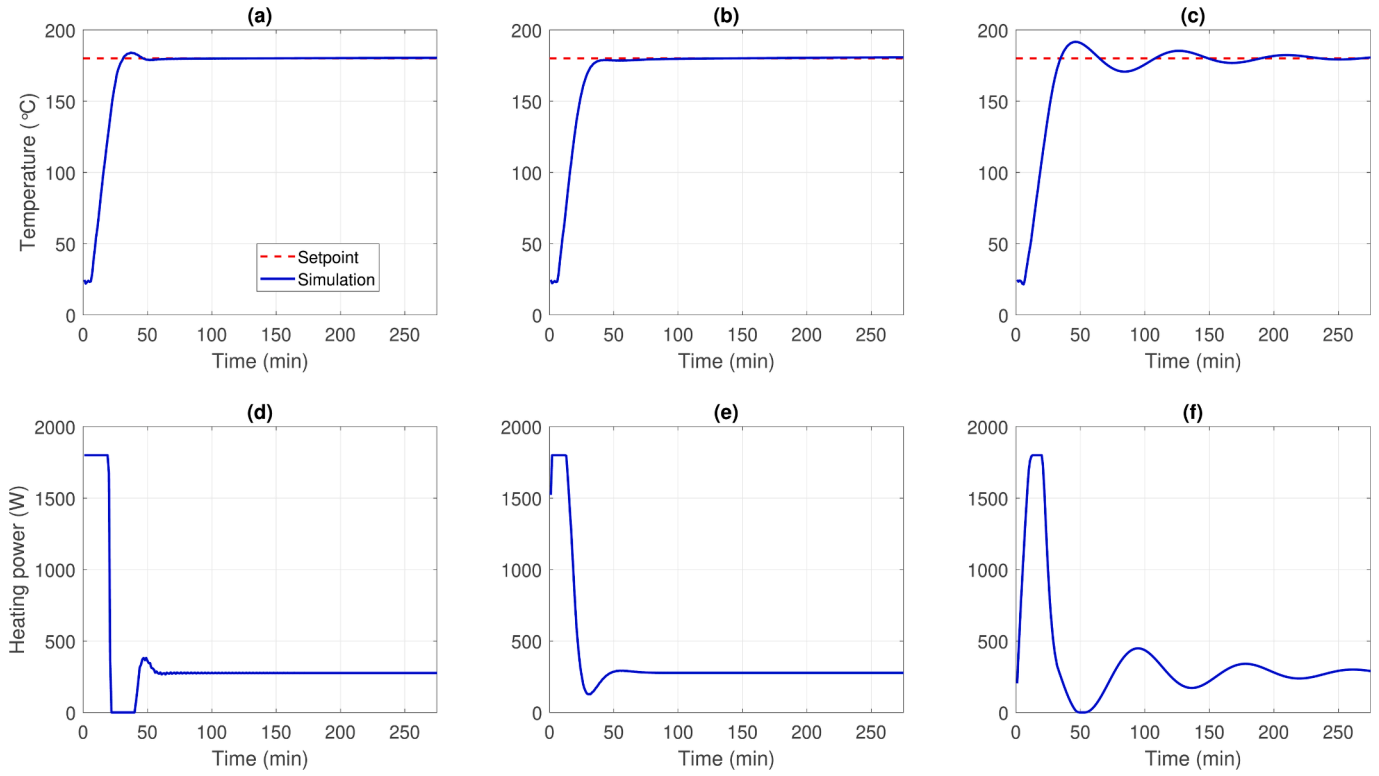

Fig. 12. Reactor temperature (top) and heating power (bottom) in three simulations. Graphs (a) and (d) show the case where *MAPE* was minimised, whereas overshoot was minimised in graphs (b) and (e), and energy consumption was minimised in graphs (c) and (f).

loop output, was defined by MPC that did the predictions by using a control model. The process was simulated with 31 models and all the controller settings described in Table 3 were tested.

Fig. 10 shows the lowest mean values for three performance metrics in the simulations with different control models. The optimal combination of control parameter values was different for each model. The values of the performance metrics were calculated from the periods at target temperature defined by the actual laboratory experiments. Unsuccessful controller settings were removed from the simulation results: If the mean value for any metric was higher than the maximum in 31 laboratory experiments, the results of that setting were removed.

Based on the results, the control model with the order of 7 was generally the best, because it reached the lowest relative error (*MAPE* = 0.56%), the lowest overshoot (2.50 °C), and the second lowest energy consumption at target temperature (1.32 kWh or 40.86 kWh for one kilogram of hydrochar produced). The lowest energy consumption was reached with the model that had an order of 1 (1.27 kWh or 39.32 kWh/kg). However, that model suffered especially from the high overshoot, which indicates that the control performance was inferior. Interestingly, the model with the best accuracy in model identification (order = 5) was among the three worst models based on all the metrics. This indicates that selecting a model without simulating its use in control, could lead into a poor selection. Then again, the missing values in Fig. 10 for the models with the orders of 6, 8, and 9 can be partially explained by inappropriate controller settings, such as a too short prediction horizon, as indicated by additional testing not illustrated here. Therefore, the control model candidates must be tested in simulations with the selected control settings to determine their suitability for the intended use.

Fig. 11 illustrates the effects of control parameters (w_{mr}, w_o, ne) on the selected performance metrics. The values of metrics represent the mean values of 31 process simulations for different control settings. The control model with the order of 7 was applied in these simulations. In each shown boxplot, the parameter value in question was kept fixed while the other parameter values were changed. The unsuccessful tests were removed with the same approach as above. The boxplots contain a varying number of samples.

Table 4
Values of performance metrics in three optimised cases and corresponding control settings. The process model of experiment 14 and control model with order of 7 were used with process settings $t = 4$ h and $T = 180$ °C.

		Optimal *MAPE*	Optimal *O*	Optimal *E*
Results				
	MAPE(%)	0.19	0.29	1.80
	O(°C)	4.07	0.77	11.63
	E(kWh)	1.09	1.10	1.02
Settings				
	w_{mr}	0.1	1	1
	w_o	0.8	1	0.2
	ne	20	20	14

The results indicate that the prediction horizon had the greatest effect on the performance metrics. The deviation from the setpoint (*MAPE*) and overshoot generally decreased with an increasing prediction horizon whereas the energy consumption increased. The other two control parameters had weak correlations with the performance metrics.

The full ranges of mean values were 0.56–3.41% for *MAPE*, 2.50–19.41 °C for overshoot, and 1.32–1.39 kWh for energy consumption. The maximum values were thus 610%, 780%, and 5% higher than the minimum values, respectively. This suggests that the control effects were relatively minuscule on the energy consumption on average but substantial on the other two metrics.

The selection of control settings, such as the prediction horizon, appears to be a trade-off between the energy consumption and the tracking error. However, the energy consumption seems to be largely dependent on the processing time and temperature setpoint, as illustrated in Sections 3.1 and 3.2. Therefore, the small tracking error, as indicated by low *MAPE* and overshoot, can be a practical aim for the control optimisation.

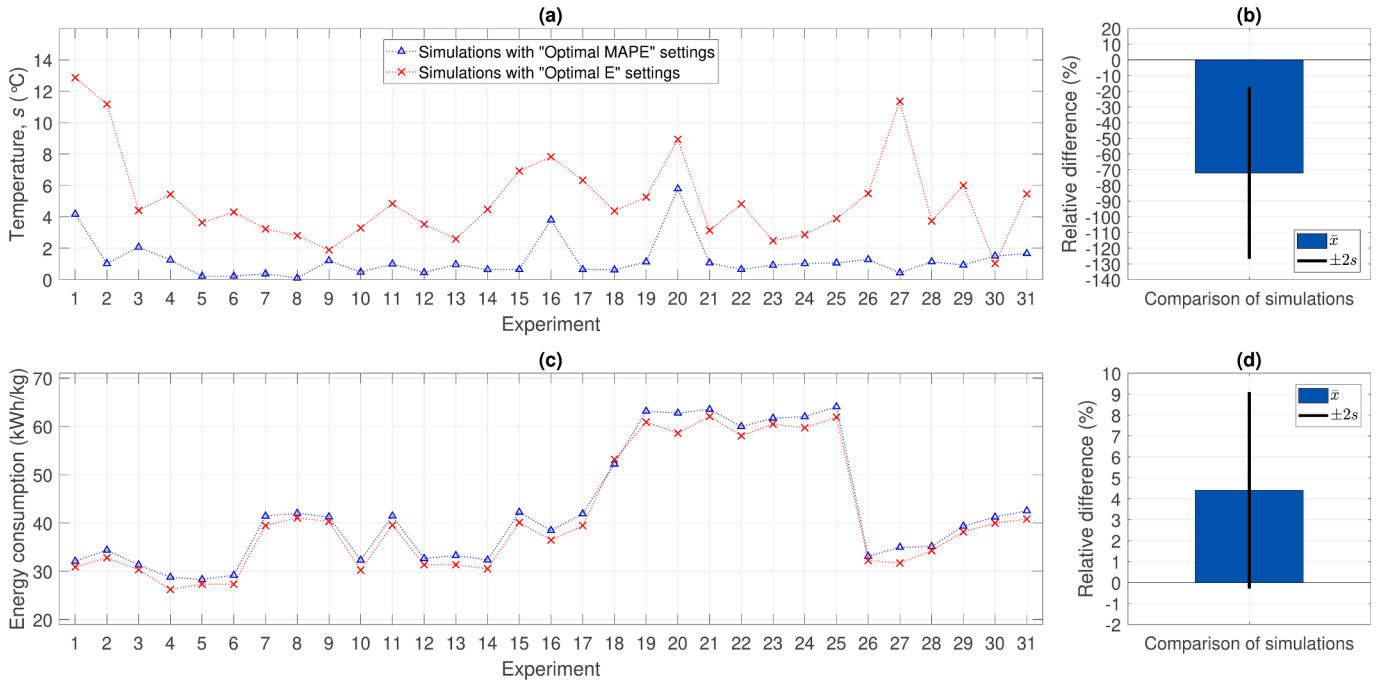

Fig. 13. (a) Standard deviations of reactor temperature in 31 experiments, (b) relative difference between "Optimal *MAPE*" and "Optimal *E*" settings for standard deviations of reactor temperatures, (c) specific energy consumption values, and (d) relative difference between "Optimal *MAPE*" and "Optimal *E*" settings for specific energy consumption values.

3.5. Simulation cases with optimal controller settings

Fig. 12 shows three simulation cases where the control model with the order of 7 was applied together with the process model of experiment 14 (where $t = 4$ h, $T = 180$ °C). The controller settings (w_{mr}, w_o, and ne together) were selected based on the minimum mean *MAPE*, overshoot, and energy consumption in 31 process simulations. Table 4 presents the values of the performance metrics in the simulation cases together with the optimised control settings. The matrices of both models are given in Appendix B.

The results illustrate the effect of heating on the reactor temperature. In the start, the reactor was heated with high power (1.8 kW) to increase the temperature level towards the setpoint. However, the heating behaviour near the room temperature in the identified models is unrealistic, while the temperature increases there even without heating, which can be tested with the models described in Appendix B Therefore, the behaviour closer to the setpoint is more relevant.

The heating power dropped after the initial heating part and the

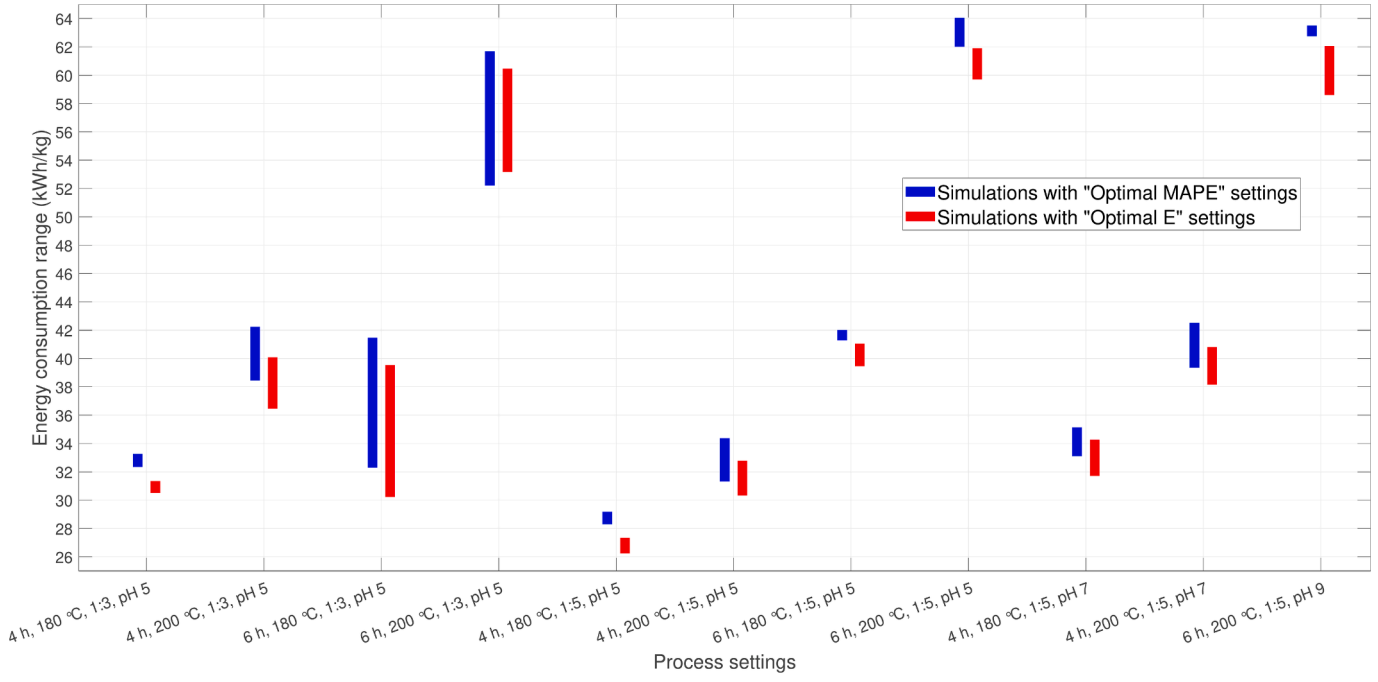

Fig. 14. Variation of specific energy consumption based on repetitions of specific process settings.

operation had differences between the cases thereafter. In cases with the optimal *MAPE* and overshoot, the power settled close to 280 W after the drop. The change was slightly smoother in the case of overshoot optimisation. The prediction horizon was 20 min long in both, but the other two control parameters had smaller values for *MAPE* optimisation. To optimise the energy consumption, the reactor temperature was allowed to swing around the setpoint, as shown in graph (c). This was caused by the fluctuating heating power, as shown in graph (f). In this case, the values of ne and w_o were smaller than in the other two optimised cases. With a short prediction horizon (ne), the MPC controller adapted to the slow dynamics of the process more imperfectly, and additionally, the low output weight (w_o) allowed deviations from the setpoint.

3.6. Variation of reactor temperature and energy consumption

Additional simulations were performed with the 31 process models to study the variation of reactor temperature and energy consumption together. The control model shown in Appendix B and "Optimal *MAPE*" and "Optimal *E*" settings shown in Table 4 were used in MPC. Energy consumption was normalised by dividing it with the dry mass of produced hydrochar, shown in Appendix A In the simulations, it was assumed that the same yield of hydrochar was achieved as in the laboratory experiments.

Fig. 13a shows the standard deviations of reactor temperature from the periods after temperature setpoint was reached the first time in the experiments. The lowest standard deviations (with its mean 1.24 °C in the range of 0.10–5.78 °C) were reached with "Optimal *MAPE*" setting, whereas "Optimal *E*" setting had the range of 1.03–12.86 °C (with mean 5.11 °C). Graph (b) indicates that the standard deviation of temperature was 72% smaller on average by using "Optimal *MAPE*" setting instead of "Optimal *E*" setting. On the contrary, graph (c) indicates that "Optimal *E*" setting generally resulted in lower energy consumption. Graph (d) reveals that the use of "Optimal *MAPE*" setting resulted in 4.4% higher energy consumption than "Optimal *E*" setting on average. These results suggest that a strict temperature control, which is the goal in industry to obtain high product quality and safe operation, may require a slightly higher energy consumption than control settings that allow more variation around the selected setpoint.

Fig. 14 illustrates the ranges of specific energy consumption values for all 11 process settings included in data set 1. The simulations with "Optimal *MAPE*" setting had 8.3% narrower range than the simulations with "Optimal *E*" setting on average. The broadest range with "Optimal *MAPE*" setting was 30% broader than the corresponding range with "Optimal *E*" setting (6 h, 200 °C, 1:3, pH 5), whereas the narrowest range with "Optimal *MAPE*" was 78% narrower than the range with "Optimal *E*" setting (6 h, 200 °C, 1:5, pH 9). These simulation results mainly indicate that the energy consumption of a specific process setting can be controlled accurately especially with settings that minimise the tracking error. Concluding from Figs. 13 and 14 together, MPC and dynamic models can enable accurate process control and detailed predictability to the energy consumption of HTC as well.

3.7. Discussion

Energy consumption in hydrothermal carbonisation is strongly correlated with processing time and temperature setpoint, as shown in Fig. 14 (26–35, 30–42, and 52–64 kWh/kg for 4 h in 180 °C, 6 h in 180 °C, and 6 h in 200 °C, respectively) and can be inferred from literature [13,21,54]. The simulations presented in Sections 3.4–3.6 also indicated that the energy consumption was affected by the control actions during processing, which seems a rather unstudied topic for HTC [37]. However, it seems that the effect on energy consumption was small (the relative differences between control settings were $\bar{x} = 4.4\%$ in Fig. 13). Therefore, the focus of control optimisation could be at minimising the deviation of the controlled variable, such as reactor temperature, from its setpoint. This was well achieved in the simulations, as shown in Section 3.4, where the mean value of *MAPE* as low as 0.56% was achieved.

Accurate models were identified with the chosen identification method, as shown in Section 3.3, where the most accurate model had *RMSE* in the range of 2.19–6.38 °C. Interestingly, the results in Section 3.4 clearly showed that the most accurate model was not the optimal one from the control perspective (see Fig. 10). Therefore, it seems that the exhaustive simulations with different models, identified based on the data of different laboratory experiments, were necessary to obtain the most optimal models for control. The versatile data of multiple laboratory experiments were essential for the model validation purpose. Furthermore, the results of process simulations (e.g. Fig. 12) suggest that the mismatch between process and control models did not cause major complications for the process control, highlighting the potential of this modelling approach also for practical applications.

The presented analysis has many areas that could benefit from additional research. The analysis was based on one laboratory set-up only which means that the results are case-specific. Laboratory-scale reactors are not representative of industrial-scale reactors [13], and therefore, the results cannot be directly scaled to a commercial setting, where semi-continuous, continuous, or multi-batch HTC processes can be used [12,55,56]. However, obviously, the presented data-driven dynamic modelling approach is not limited to batch reactors. The experimental planning for the laboratory experiments was done primarily for producing hydrochar at specific synthesis conditions. The identification of process dynamics was therefore a secondary target in experimental planning. Additional tests in other operational areas and situations could further improve the identification of process dynamics. Moreover, the temperature variation during processing could be further studied from the perspective of its effects on hydrochar properties to light up the connection between process control and hydrochar quality. In addition, the energy consumption was estimated indirectly from a process variable (control loop output), which was not validated with a real-time synchronized energy consumption measurement. However, the validation based on total energy consumption shown in Section 3.1 indicated that the difference between the medians of measurements and estimates for a specific process setting was 11.5% at maximum, which could be mainly explained by the unexpected variation of the power meter readings.

Finally, this study can advance the development of digital twins for hydrothermal carbonisation [57]. The results suggested that simulations with the identified dynamic models could provide accurate results for production planning, where also the energy consumption must be considered. Moreover, the process simulations can be conducted in real-time on the side of the physical process and return the control values there in case appropriate equipment and connections between the physical and digital twins exist.

4. Conclusions

State-space models were identified and used in simulations for predicting reactor temperature changes based on the control values of reactor heating in hydrothermal carbonisation. The results showed that accurate control models were identified with this approach which also enabled estimating the energy consumption in real-time. The prediction horizon length in MPC was statistically the most significant control parameter affecting the selected performance metrics. The simulations clearly indicated that the reactor temperature could be controlled accurately, especially when long prediction horizons (e.g. 20 min) were applied. To control the energy consumption during processing, the appropriate adjustment of temperature setpoint and processing time proved to be highly important. In conclusion, the applied dynamic modelling approach can enable accurate process control and energy consumption predictions for hydrothermal carbonisation, which can ease the pursuit for energy efficient hydrothermal carbonisation.

Table A1
Process settings for the laboratory experiments and hydrochar mass in data sets analysed.

Data set 1						Data set 2					
Exp.	T (°C)	t (h)	pH	Water (ml)	Hydrochar mass (g)	Exp.	T (°C)	t (h)	pH	Water (ml)	Hydrochar mass (g)
1	200	4	5	230.3	32.71	32	200	4	9	230.3	31.52
2	200	4	5	230.3	32.25	33	200	4	9	230.3	31.58
3	200	4	5	230.3	32.40	34	200	4	9	202.5	31.95
4	180	4	5	230.3	33.26	35	200	4	9	202.5	31.81
5	180	4	5	230.3	33.13	36	200	4	9	202.5	31.85
6	180	4	5	230.3	33.45	37	180	4	9	202.5	32.03
7	180	6	5	230.3	33.11	38	180	4	9	202.5	32.51
8	180	6	5	230.3	33.59	39	180	4	9	202.5	31.81
9	180	6	5	230.3	33.44	40	180	4	9	230.3	32.13
10	180	6	5	202.5	33.67	41	180	4	9	230.3	32.03
11	180	6	5	202.5	32.98	42	180	4	9	230.3	31.98
12	180	4	5	202.5	33.50	43	180	4	7	202.5	32.16
13	180	4	5	202.5	33.34	44	180	4	7	202.5	31.88
14	180	4	5	202.5	33.59	45	180	4	7	202.5	31.56
15	200	4	5	202.5	32.75	46	200	4	7	202.5	31.23
16	200	4	5	202.5	32.12	47	200	4	7	202.5	31.61
17	200	4	5	202.5	32.03	48	200	4	7	202.5	31.75
18	200	6	5	202.5	32.25	49	200	6	7	202.5	31.71
19	200	6	5	230.3	31.74	50	200	6	7	202.5	31.44
20	200	6	9	230.3	31.40	51	200	6	7	202.5	31.98
21	200	6	9	230.3	31.48	52	180	6	7	202.5	32.03
22	200	6	5	202.5	32.38	53	180	6	7	202.5	32.12
23	200	6	5	202.5	31.23	54	180	6	7	202.5	32.41
24	200	6	5	230.3	31.43						
25	200	6	5	230.3	31.82						
26	180	4	7	230.3	31.92						
27	180	4	7	230.3	32.23						
28	180	4	7	230.3	32.14						
29	200	4	7	230.3	31.45						
30	200	4	7	230.3	31.67						
31	200	4	7	230.3	31.17						

CRediT authorship contribution statement

Riku-Pekka Nikula: Writing – review & editing, Writing – original draft, Visualization, Validation, Software, Methodology, Investigation, Formal analysis, Data curation, Conceptualization. **Sajad Ahmadi:** Writing – review & editing, Visualization, Validation, Resources, Methodology, Investigation. **Velma Beri Kimbi Yaah:** Writing – review & editing, Validation, Resources, Methodology, Investigation. **Hafiz Haq:** Writing – review & editing. **Ville Tuomi:** Writing – review & editing. **Mika Ruusunen:** Writing – review & editing, Supervision, Project administration, Funding acquisition, Conceptualization.

Declaration of competing interest

The authors declare that they have no known competing financial interests or personal relationships that could have appeared to influence the work reported in this paper.

Acknowledgements

The ministry of agriculture and forestry of Finland is acknowledged for funding the Biodigi project VN/28442/2021-MMM-2. Kiertokaari Oy (Oulu, Finland) is acknowledged for providing the construction wood waste as raw material for the laboratory experiments.

Appendix A

The process settings and the dry mass of the produced hydrochar are shown in Table A.1. Biomass-to-water ratio 1:3 is associated with 202.5 ml water volume, whereas ratio 1:5 is associated with 230.3 ml volume.

Appendix B

The models applied in Section 3.5 are described here. The state, input, output, and feedthrough matrices of the control model (order = 7) were

$$A = \begin{bmatrix} 1.011 & 0.4303 & -2.961 & 1.826 & -5.012 & -0.1501 & 0.6251 \\ -0.0017 & 0.8883 & 0.5999 & 0.168 & 0.3226 & -0.2211 & -0.2917 \\ -3.051e-05 & -0.01878 & 0.8947 & -0.6672 & 0.07529 & 0.106 & -0.1946 \\ 2.047e-05 & 0.0002809 & 0.07518 & 0.5208 & -0.7185 & 0.4062 & 0.624 \\ 1.629e-05 & 0.00927 & 0.09935 & 0.2198 & 0.5762 & 0.06461 & 0.1557 \\ 1.406e-05 & -0.001028 & 0.008588 & -0.2199 & 0.08244 & -0.5811 & 0.7746 \\ -8.797e-06 & -1.833e-05 & 0.0006867 & 0.02356 & -0.5612 & -0.5401 & -0.23 \end{bmatrix}$$

$$B = \begin{bmatrix} 0.0941 \\ 0.0689 \\ 0.002555 \\ -0.003367 \\ 0.003992 \\ -0.007316 \\ 0.0304 \end{bmatrix}$$

$$C = \begin{bmatrix} 0.3002 & -0.5528 & 0.4873 & 0.4247 & 0.1984 & -0.2103 & -0.1228 \end{bmatrix}$$

$$D = 0$$

The initial state of the control model was

$$x = \begin{bmatrix} 123.2761 \\ 45.5854 \\ 18.7501 \\ -5.7127 \\ -11.6069 \\ 0.2567 \\ -6.4761 \end{bmatrix}$$

The matrices of the process model (order = 9) were

$$A = \begin{bmatrix} 0.9919 & -0.001262 & -0.02938 & 0.003449 & 0.04398 & -0.002825 & 0.000694 & 0.0006799 & -0.02849 \\ -0.1611 & 0.9867 & -0.05152 & -0.0286 & 0.02192 & 0.02124 & -0.02065 & 0.02384 & -0.0546 \\ 0.1177 & 0.1042 & 0.7001 & 0.2025 & 0.426 & 0.03201 & -0.04739 & 0.05618 & 0.02723 \\ -0.02649 & -0.005014 & 0.01736 & 0.1846 & 0.3114 & 0.3844 & 0.1491 & -1.277 & 0.4154 \\ 0.09207 & 0.02744 & -0.2836 & -0.7297 & 0.2579 & -0.07572 & 0.01759 & -0.109 & 0.1835 \\ 0.03252 & 0.02728 & -0.1256 & 0.2325 & -0.02985 & -0.5698 & -0.632 & -0.3224 & 0.02197 \\ 0.003197 & -0.04556 & 0.1037 & -0.2017 & -0.1111 & 0.6353 & -0.7077 & -0.05844 & -0.117 \\ -0.04317 & -0.02173 & 0.2142 & -0.2591 & -0.09102 & -0.3538 & -0.01861 & -0.3696 & -0.4175 \\ 0.01318 & 0.02072 & 0.06834 & -0.1043 & -0.3169 & -0.02166 & 0.004176 & -0.04101 & 0.3327 \end{bmatrix}$$

$$B = \begin{bmatrix} 0.01162 \\ 0.02011 \\ -0.075 \\ 0.09092 \\ -0.06879 \\ 0.03178 \\ 0.003286 \\ -0.04275 \\ 0.02099 \end{bmatrix}$$

$$C = \begin{bmatrix} 1742 & -1017 & -41.81 & -7.52 & 42.09 & -11.64 & 18.29 & -14.12 & 17.34 \end{bmatrix}$$

$$D = 0$$

The initial state of the process model was

$$x = \begin{bmatrix} 36.9816 \\ 63.8746 \\ -247.2324 \\ 298.6018 \\ -224.2134 \\ 113.3537 \\ 6.5314 \\ -150.8753 \\ 58.7778 \end{bmatrix}$$

Data availability

The raw data required to reproduce the above findings are available to download from https://doi.org/10.23729/6ad31974-8511-4f3c-9487-58b8c3e23457.

References

[1] Kumar M, Olajire Oyedun A, Kumar A. A review on the current status of various hydrothermal technologies on biomass feedstock. Renew Sustain Energy Rev 2018; 81:1742–70. https://doi.org/10.1016/j.rser.2017.05.270.

[2] Masoumi S, Borugadda VB, Nanda S, Hydrochar DAK. A review on its production technologies and applications. Catalysts 2021;11. https://doi.org/10.3390/catal11080939.

[3] Mäkelä M, Benavente V, Fullana A. Hydrothermal carbonization of lignocellulosic biomass: Effect of process conditions on hydrochar properties. Appl Energy 2015; 155:576–84. https://doi.org/10.1016/j.apenergy.2015.06.022.

[4] López R, González-Arias J, Pereira FJ, Fernández C, Cara-Jiménez J. A techno-economic study of HTC processes coupled with power facilities and oxy-combustion systems. Energy 2021;219. https://doi.org/10.1016/j.energy.2020.119651.

[5] Funke A, Ziegler F. Hydrothermal carbonization of biomass: A summary and discussion of chemical mechanisms for process engineering. Biofuels Bioprod Biorefin 2010;4:160–77. https://doi.org/10.1002/bbb.198.

[6] Kumar A, Saini K, Bhaskar T. Hydochar and biochar: Production, physicochemical properties and techno-economic analysis. Bioresour Technol 2020;310. https://doi.org/10.1016/j.biortech.2020.123442.

[7] Escala M, Zumbühl T, Koller C, Junge R, Krebs R. Hydrothermal carbonization as an energy-efficient alternative to established drying technologies for sewage sludge: A feasibility study on a laboratory scale. Energy Fuel 2013;27:454–60. https://doi.org/10.1021/ef3015266.

[8] Islam MA, Limon MSH, Romić M. Islam MdA. Hydrochar-based soil amendments for agriculture: a review of recent progress. Arab J Geosci 2021;14. https://doi.org/10.1007/s12517-020-06358-8.

[9] Kimbi Yaah VB, Zbair M, Botelho de Oliveira S, Ojala S. Hydrochar-derived adsorbent for the removal of diclofenac from aqueous solution. Nanotechnology for Environmental Engineering 2021;6. https://doi.org/10.1007/s41204-020-00099-5.

[10] Naisse C, Girardin C, Lefevre R, Pozzi A, Maas R, Stark A, et al. Effect of physical weathering on the carbon sequestration potential of biochars and hydrochars in soil. GCB Bioenergy 2015;7:488–96. https://doi.org/10.1111/gcbb.12158.

[11] Hu B, Wang K, Wu L, Yu S-H, Antonietti M, Titirici M-M. Engineering carbon materials from the hydrothermal carbonization process of biomass. Adv Mater 2010;22:813–28. https://doi.org/10.1002/adma.200902812.

[12] Yu S, He J, Zhang Z, Sun Z, Xie M, Xu Y, et al. Towards Negative Emissions: Hydrothermal Carbonization of Biomass for Sustainable Carbon Materials. Adv Mater 2024;36. https://doi.org/10.1002/adma.202307412.

[13] Sangaré D, Moscosa-Santillan M, Aragón Piña A, Bostyn S, Belandria V, Gökalp I. Hydrothermal carbonization of biomass: experimental study, energy balance, process simulation, design, and techno-economic analysis. Biomass Convers Biorefin 2024;14:2561–76. https://doi.org/10.1007/s13399-022-02484-3.

[14] Picone A, Volpe M, Malik W, Volpe R, Messineo A. Role of reaction parameters in hydrothermal carbonization with process water recirculation: Hydrochar recovery enhancement and energy balance. Biomass Bioenergy 2024;181. https://doi.org/10.1016/j.biombioe.2024.107061.

[15] Ischia G, Berge ND, Bae S, Marzban N, Román S, Farru G, et al. Advances in Research and Technology of Hydrothermal Carbonization: Achievements and Future Directions. Agronomy 2024;14. https://doi.org/10.3390/agronomy14050955.

[16] Medina-Martos E, Istrate IR, Villamil JA, Gálvez-Martos JL, Dufour J, Mohedano ÁF. Techno-economic and life cycle assessment of an integrated hydrothermal carbonization system for sewage sludge. J Clean Prod 2020;277. https://doi.org/10.1016/j.jclepro.2020.122930.

[17] Saari J, Sermyagina E, Kaikko J, Vakkilainen E, Sergeev V. Integration of hydrothermal carbonization and a CHP plant: Part 2 –operational and economic analysis. Energy 2016;113:574–85. https://doi.org/10.1016/j.energy.2016.06.102.

[18] Saari J, Sermyagina E, Kuparinen K, Lipiäinen S, Kaikko J, Hamaguchi M, et al. Improving Kraft Pulp Mill Energy Efficiency through Low-Temperature Hydrothermal Carbonization of Biological Sludge. Energies (basel) 2022;15:6188. https://doi.org/10.3390/en15176188.

[19] Funke A, Ziegler F. Heat of reaction measurements for hydrothermal carbonization of biomass. Bioresour Technol 2011;102:7595–8. https://doi.org/10.1016/j.biortech.2011.05.016.

[20] Śliz M, Wilk M. A comprehensive investigation of hydrothermal carbonization: Energy potential of hydrochar derived from Virginia mallow. Renew Energy 2020; 156:942–50. https://doi.org/10.1016/j.renene.2020.04.124.

[21] Heidari M, Salaudeen S, Arku P, Acharya B, Tasnim S, Dutta A. Development of a mathematical model for hydrothermal carbonization of biomass: Comparison of experimental measurements with model predictions. Energy 2021;214. https://doi.org/10.1016/j.energy.2020.119020.

[22] Li L, Flora JRV, Berge ND. Predictions of energy recovery from hydrochar generated from the hydrothermal carbonization of organic wastes. Renew Energy 2020;145:1883–9. https://doi.org/10.1016/j.renene.2019.07.103.

[23] Sharma HB, Panigrahi S, Dubey BK. Hydrothermal carbonization of yard waste for solid bio-fuel production: Study on combustion kinetic, energy properties, grindability and flowability of hydrochar. Waste Manag 2019;91:108–19. https://doi.org/10.1016/j.wasman.2019.04.056.

[24] Ischia G, Fiori L. Hydrothermal Carbonization of Organic Waste and Biomass: A Review on Process, Reactor, and Plant Modeling. Waste Biomass Valorization 2021;12:2797–824. https://doi.org/10.1007/s12649-020-01255-3.

[25] Hämäläinen H, Ruusunen M. Identification of a supercritical fluid extraction process for modelling the energy consumption. Energy 2022;252. https://doi.org/10.1016/j.energy.2022.124033.

[26] Aragon-Briceño C, Pożarlik A, Bramer E, Brem G, Wang S, Wen Y, et al. Integration of hydrothermal carbonization treatment for water and energy recovery from organic fraction of municipal solid waste digestate. Renew Energy 2022;184: 577–91. https://doi.org/10.1016/j.renene.2021.11.106.

[27] Danso-Boateng E, Shama G, Wheatley AD, Martin SJ, Holdich RG. Hydrothermal carbonisation of sewage sludge: Effect of process conditions on product characteristics and methane production. Bioresour Technol 2015;177:318–27. https://doi.org/10.1016/j.biortech.2014.11.096.

[28] Volpe M, Goldfarb JL, Fiori L. Hydrothermal carbonization of Opuntia ficus-indica cladodes: Role of process parameters on hydrochar properties. Bioresour Technol 2018;247:310–8. https://doi.org/10.1016/j.biortech.2017.09.072.

[29] Gallifuoco A, Taglieri L, Scimia F, Papa AA, Di Giacomo G. Hydrothermal carbonization of Biomass: New experimental procedures for improving the industrial Processes. Bioresour Technol 2017;244:160–5. https://doi.org/10.1016/j.biortech.2017.07.114.

[30] Sermyagina E, Saari J, Kaikko J, Vakkilainen E. Hydrothermal carbonization of coniferous biomass: Effect of process parameters on mass and energy yields. J Anal Appl Pyrolysis 2015;113:551–6. https://doi.org/10.1016/j.jaap.2015.03.012.

[31] Li L, Flora JRV, Caicedo JM, Berge ND. Investigating the role of feedstock properties and process conditions on products formed during the hydrothermal carbonization of organics using regression techniques. Bioresour Technol 2015; 187:263–74. https://doi.org/10.1016/j.biortech.2015.03.054.

[32] Vallejo F, Díaz-Robles LA, Vega R, Cubillos F. A novel approach for prediction of mass yield and higher calorific value of hydrothermal carbonization by a robust multilinear model and regression trees. J Energy Inst 2020;93:1755–62. https://doi.org/10.1016/j.joei.2020.03.006.

[33] Djandja OS, Salami AA, Wang ZC, Duo J, Yin LX, Duan PG. Random forest-based modeling for insights on phosphorus content in hydrochar produced from hydrothermal carbonization of sewage sludge. Energy 2022;245. https://doi.org/10.1016/j.energy.2022.123295.

[34] Li J, Zhu X, Li Y, Tong YW, Ok YS, Wang X. Multi-task prediction and optimization of hydrochar properties from high-moisture municipal solid waste: Application of machine learning on waste-to-resource. J Clean Prod 2021;278. https://doi.org/10.1016/j.jclepro.2020.123928.

[35] Ismail HY, Shirazian S, Skoretska I, Mynko O, Ghanim B, Leahy JJ, et al. ANN-Kriging hybrid model for predicting carbon and inorganic phosphorus recovery in hydrothermal carbonization. Waste Manag 2019;85:242–52. https://doi.org/10.1016/j.wasman.2018.12.044.

[36] Katongtung T, Prasertpong P, Sukpancharoen S, Sinthupinyo S, Tippayawong N. Predictive modeling for multifaceted hydrothermal carbonization of biomass. J Environ Chem Eng 2024;12. https://doi.org/10.1016/j.jece.2024.114071.

[37] Li J, Suvarna M, Li L, Pan L, Pérez-Ramírez J, Ok YS, et al. A review of computational modeling techniques for wet waste valorization: Research trends and future perspectives. J Clean Prod 2022;367:133025. https://doi.org/10.1016/j.jclepro.2022.133025.

[38] Ubene M, Heidari M, Dutta A. Computational Modeling Approaches of Hydrothermal Carbonization: A Critical Review. Energies (basel) 2022;15:2209. https://doi.org/10.3390/en15062209.

[39] Van Overschee P, De Moor B. N4SID: Subspace algorithms for the identification of combined deterministic stochastic systems. Automatica 1994;30:75–93.

[40] Saha N, Saba A, Reza MT. Effect of hydrothermal carbonization temperature on pH, dissociation constants, and acidic functional groups on hydrochar from cellulose and wood. J Anal Appl Pyrolysis 2019;137:138–45. https://doi.org/10.1016/j.jaap.2018.11.018.

[41] Schwenzer M, Ay M, Bergs T, Abel D. Review on model predictive control: an engineering perspective. Int J Adv Manuf Technol 2021;117:1327–49. https://doi.org/10.1007/s00170-021-07682-3.

[42] Chachuat B, Srinivasan B, Bonvin D. Adaptation strategies for real-time optimization. Comput Chem Eng 2009;33:1557–67. https://doi.org/10.1016/j.compchemeng.2009.04.014.

[43] Liikkanen LA, Nieminen T. Comparison of End-User Electric Power Meters for Accuracy. Helsinki 2009.

[44] Ljung L. System Identification: Theory for the User. Second Edition. New Jersey: Prentice Hall; 1999.

[45] Larimore WE. Canonical variate analysis in identification, filtering, and adaptive control. Proceedings of the 29th IEEE Conference on Decision and Control, vol. 2, Publ by IEEE; 1990, p. 596–604. Doi: 10.1109/cdc.1990.203665.

[46] Jansson M. Subspace identification and ARX modeling. IFAC Proceedings Volumes 2003;36:1585–90. https://doi.org/10.1016/S1474-6670(17)34986-8.

[47] Verhaegen M. Identification of the deterministic part of MIMO state space models given in innovations form from input-output data. Automatica 1994;30:61–74. https://doi.org/10.1016/0005-1098(94)90229-1.

[48] Bequette BW. Process Control: Modeling, Design, and Simulation. Prentice Hall; 2003.

[49] Alhajeri M, Soroush M. Tuning Guidelines for Model-Predictive Control. Ind Eng Chem Res 2020;59:4177–91. https://doi.org/10.1021/acs.iecr.9b05931.

[50] Binder BJT, Johansen TA, Imsland L. Improved predictions from measured disturbances in linear model predictive control. J Process Control 2019;75:86–106. https://doi.org/10.1016/j.jprocont.2019.01.007.

[51] Kadlec P, Grbić R, Gabrys B. Review of adaptation mechanisms for data-driven soft sensors. Comput Chem Eng 2011;35:1–24. https://doi.org/10.1016/j.compchemeng.2010.07.034.

[52] Hewing L, Wabersich KP, Menner M, Zeilinger MN. Learning-based model predictive control: toward safe learning in control. Annu Rev Control Robot Auton Syst 2020;3:269–96. https://doi.org/10.1146/annurev-control-090419.

[53] Rawlings JB, Mayne DQ, Diehl MM. Model Predictive Control: Theory, Computation, and Design. 2nd Edition. Madison: Nob Hill Publishing; 2017.

[54] McGaughy K, Toufiq RM. Hydrothermal carbonization of food waste: simplified process simulation model based on experimental results. Biomass Convers Biorefin 2018;8:283–92. https://doi.org/10.1007/s13399-017-0276-4.

[55] Ischia G, Castello D, Orlandi M, Miotello A, Rosendahl LA, Fiori L. Waste to biofuels through zero-energy hydrothermal solar plants: Process design. Chem Eng Trans 2020;80:7–12. https://doi.org/10.3303/CET2080002.
[56] Ho TTT, Nadeem A, Choe K. A Review of Upscaling Hydrothermal Carbonization. Energies (basel) 2024;17. https://doi.org/10.3390/en17081918.
[57] Tao F, Zhang H, Liu A, Nee AYC. Digital Twin in Industry: State-of-the-Art. IEEE Trans Industr Inform 2019;15:2405–15. https://doi.org/10.1109/TII.2018.2873186.